THE JOURNAL OF BIOLOGICAL CHEMISTRY
Vol. 280, No. 4, Issue of January 28, pp. 2471–2480, 2005
Printed in U.S.A.

Amyloid-β Protofibrils Differ from Amyloid-β Aggregates Induced in Dilute Hexafluoroisopropanol in Stability and Morphology*

Received for publication, September 13, 2004, and in revised form, October 25, 2004
Published, JBC Papers in Press, November 4, 2004, DOI 10.1074/jbc.M410553200

Michael R. Nichols‡§, Melissa A. Moss‡¶, Dana Kim Reed‡, Stephanie Cratic-McDaniel‖, Jan H. Hoh‖, and Terrone L. Rosenberry‡**

From the ‡Department of Neuroscience, Mayo Clinic College of Medicine, Jacksonville, Florida 32224 and the ‖Department of Physiology, The Johns Hopkins University School of Medicine, Baltimore, Maryland 21205

The brains of Alzheimer's disease (AD) patients contain large numbers of amyloid plaques that are rich in fibrils composed of 40- and 42-residue amyloid-β (Aβ) peptides. Several lines of evidence indicate that fibrillar Aβ and especially soluble Aβ aggregates are important in the etiology of AD. Recent reports also stress that amyloid aggregates are polymorphic and that a single polypeptide can fold into multiple amyloid conformations. Here we demonstrate that Aβ-(1–40) can form soluble aggregates with predominant β-structures that differ in stability and morphology. One class of aggregates involved soluble Aβ protofibrils, prepared by vigorous overnight agitation of monomeric Aβ-(1–40) at low ionic strength. Dilution of these aggregation reactions induced disaggregation to monomers as measured by size exclusion chromatography. Protofibril concentrations monitored by thioflavin T fluorescence decreased in at least two kinetic phases, with initial disaggregation (rate constant ~1 h^{-1}) followed by a much slower secondary phase. Incubation of the reactions without agitation resulted in less disaggregation at slower rates, indicating that the protofibrils became progressively more stable over time. In fact, protofibrils isolated by size exclusion chromatography were completely stable and gave no disaggregation. A second class of soluble Aβ aggregates was generated rapidly (<10 min) in buffered 2% hexafluoroisopropanol (HFIP). These aggregates showed increased thioflavin T fluorescence and were rich in β-structure by circular dichroism. Electron microscopy and atomic force microscopy revealed initial globular clusters that progressed over several days to soluble fibrous aggregates. When diluted out of HFIP, these aggregates initially were very unstable and disaggregated completely within 2 min. However, their stability increased as they progressed to fibers. Relative to Aβ protofibrils, the HFIP-induced aggregates seeded elongation by Aβ monomer deposition very poorly. The techniques used to distinguish these two classes of soluble Aβ aggregates may be useful in characterizing Aβ aggregates formed *in vivo*.

Alzheimer's disease (AD)[1] is one of a number of diseases in which proteins form amyloid aggregates. The brains of patients with AD contain large numbers of amyloid deposits in the form of senile plaques (1). The amyloid core of these plaques contains interwoven fibrils that are composed of 40- and 42-residue peptides (2, 3), denoted Aβ-(1–40) and Aβ-(1–42). These peptides are produced by cleavage of cellular amyloid precursor protein by two proteases called β- and γ-secretase (reviewed in Ref. 4). As originally suggested by the amyloid cascade hypothesis (5), it appears likely that Aβ aggregates are important in the etiology of AD. The most striking evidence supporting this hypothesis comes from the identification of numerous mutations linked to early onset familial AD (6). These mutations are located within the amyloid precursor protein gene or the genes for presenilins 1 and 2, which play an integral role in γ-secretase activity. All early onset familial AD mutations reported thus far increase either the level of the more amyloidogenic Aβ-(1–42) peptide (reviewed in Ref. 6) or the propensity of a mutated Aβ to form amyloid aggregates (7). Whereas early evidence suggested that Aβ fibrils initiate a cascade of events that result in neuronal cell death (8), a number of investigators now propose that soluble aggregates of Aβ (also called oligomers or protofibrils), rather than monomers or insoluble amyloid fibrils, may be responsible for synaptic dysfunction in AD (9–13). This proposal is supported by observations that soluble aggregates generated *in vitro* from synthetic Aβ-(1–40) and -(1–42) induced toxicity in cultured cells (10, 14), that soluble Aβ aggregates produced in cell culture markedly inhibited hippocampal long term potentiation in rats *in vivo* (15), and that transgenic mice expressing human Aβ show functional deficits that precede extracellular deposition of fibrillar Aβ (12, 16).

Amyloid fibrils from a number of proteins share certain structural features. They contain fully extended peptide segments that align to form β-sheets with the extended peptide strands perpendicular to and interstrand hydrogen bonds parallel to the fibril axis (17, 18). This cross-β structure may underlie common properties including the binding of dyes like thioflavin T and Congo Red and of antibodies that react with a common epitope in several amyloidogenic proteins (19, 20). However, recent reports also indicate a fascinating degree of amyloid polymorphism at the molecular level. This feature was first noted with mammalian and yeast prion proteins when it was shown that a single polypeptide can misfold into multiple amyloid conformations (21). Specifically, the yeast Sup35p

* This work was supported by awards from the American Heart Association, Florida/Puerto Rico Affiliate (to M. R. N. and M. A. M.) and by National Institutes of Health Grant 5 R25 GM64124 (to S. C.-M.). The costs of publication of this article were defrayed in part by the payment of page charges. This article must therefore be hereby marked "*advertisement*" in accordance with 18 U.S.C. Section 1734 solely to indicate this fact.

§ Present address: Dept. of Chemistry and Biochemistry, University of Missouri-St. Louis, St. Louis, MO 63121-4400.

¶ Present address: Dept. of Chemical Engineering, University of South Carolina, Columbia, SC 29208.

** To whom correspondence should be addressed: Dept. of Neuroscience, Mayo Clinic College of Medicine, 4500 San Pablo Rd., Jacksonville, FL 32224. Tel.: 904-953-7375; Fax: 904-953-7370; E-mail: rosenberry@mayo.edu.

[1] The abbreviations used are: AD, Alzheimer's disease; AFM, atomic force microscopy; BSA, bovine serum albumin; DLS, dynamic light scattering; EM, electron microscopy; HFIP, hexafluoroisopropanol; MALS, multiangle light scattering; SEC, size exclusion chromatography; TFE, trifluoroethanol; G_{M1}, monosialoganglioteraosylceramide.

prion protein was aggregated at different temperatures into amyloid conformations that could be distinguished by thermal stability and EPR spectroscopy, and infection of yeast with these different conformations led to different propagating yeast [PSI^+] strains (22, 23). Aβ fibrils also show molecular diversity. Solid state NMR measurements revealed that Aβ-(1–40), Aβ-(1–42), and Aβ-(10–35) fibrils contained in-register, parallel β-sheets (24, 25), whereas fibrils formed by the shorter peptides Aβ-(16–22), Aβ-(34–42), and Aβ-(11–25) adopted antiparallel β-strand alignments (26–28). Very recently, two types of amyloid fibrils were formed by Aβ-(1–40) following aggregation under mildly agitated or quiescent conditions, and chemical shift and line width data from solid-state NMR for 33 of the 40 residues indicated different underlying structures (29).[2]

Amyloid polymorphism is closely linked to the mechanism of Aβ fibril formation, which *in vitro* is thought to involve nucleation-dependent polymerization (31, 32). In this process, monomeric Aβ associates noncovalently to form nuclei or "seeds," which then grow into soluble protofibrils and insoluble fibrils. Nucleus formation is considered rate-limiting in this process, but this rate is highly variable even in homogeneous aqueous solutions and is sensitive to many conditions including pH, ionic strength, temperature, and agitation (33–35). If different nuclear structures form, the molecular structure of fibrils formed by polymerization will vary with the structure of the nucleus. One measure of this conformational specificity is the efficiency with which aggregates can "cross-seed," or act as seeds for elongation by another or even the same amyloidogenic polypeptide (36). Nucleation *in vivo* may be promoted by interfaces, including phospholipid membranes. Anionic phospholipid vesicles (37) as well as vesicles containing G_{M1} ganglioside (38–40) promoted Aβ binding and β-structure formation *in vitro*.

The emergence of amyloid polymorphism underscores the need for measures that would distinguish amyloid aggregates formed under different conditions. One measure that has received little attention is aggregate stability. In this report, we document the stability of Aβ-(1–40) protofibrils prepared in dilute buffer at neutral pH (35) by measuring their disaggregation rates following dilution. Isolated protofibrils became progressively more stable over time and reached a point where no disaggregation could be detected. This stability contrasted with that of Aβ aggregates generated at interfaces. We recently observed that Aβ-(1–40) aggregates formed rapidly at the interface of an aqueous solution over chloroform were relatively unstable, and their morphology differed significantly from that of Aβ-(1–40) protofibrils (41). Here we extend this characterization to Aβ-(1–40) aggregates formed in dilute hexafluoroisopropanol (HFIP). High concentrations of the fluorinated alcohols trifluoroethanol (TFE) and HFIP have been popular agents for solubilizing peptides and proteins (42). The ability of these agents to induce α-helical conformations is well known, but they also promote other types of intramolecular hydrogen bonding including turns and β-hairpins (42). In solutions that contain more than 50% TFE, Aβ (43) and the amyloidogenic protein α-synuclein (44) showed largely α-helical conformations, but in 20% TFE, both formed β-sheet aggregates at rates that were considerably faster than those in the absence of TFE. Padrick and Miranker (45) recently reported that low concentrations of HFIP (1–4%) dramatically promoted amyloid fiber formation by islet amyloid polypeptide, and their observations encouraged us to examine Aβ in dilute HFIP. We found that Aβ-(1–40) also aggregated in dilute HFIP with rates that were several orders of magnitude faster than those observed in buffer alone. These HFIP aggregates, like the Aβ aggregates formed at the chloroform-buffer interface, gave CD spectra rich in β-structure, formed globular species that progressed to fibers based on EM and AFM images, and initially disaggregated rapidly on dilution. We propose that these features provide useful criteria for investigating the polymorphism of soluble Aβ aggregates.

EXPERIMENTAL PROCEDURES

Materials—Aβ-(1–40) and Aβ-(1–42) peptides were obtained from QCB (Hopkinton, MA), from rPeptide (Athens, GA), and from the protein and peptide core facility at the Mayo Clinic (Rochester, MN). [^{3}H]HCHO was from PerkinElmer Life Sciences and ARC (St. Louis, MO); scintillation mixture (Ultima Gold) was from PerkinElmer Life Sciences; and HFIP, EDTA, bovine serum albumin, and thioflavin T were from Sigma. HFIP stocks were redistilled prior to experimental use.

Preparation of Aβ Monomers—Aβ-(1–40) peptide was obtained in lyophilized form and stored at −20 °C, desiccated until reconstitution, either in 0.1 M Tris-HCl, pH 8, at 3–4 mg/ml (460–930 μM) or in deionized water (18 megaohms; Millipore Milli-Q system) at 2.5 mg/ml (580 mM). Aliquots of the water stocks were flash frozen in ethanol/dry ice, stored at −80 °C, and thawed at room temperature when needed. Any preformed aggregates were removed from stock solutions by SEC on Superdex 75, and concentrations of Aβ (shown under "Results" to be monomeric) were determined by absorbance with a calculated extinction coefficient of 1450 cm^{-1} M^{-1} at 276 nm as previously described (35). In some experiments, Aβ peptides were radiolabeled by reductive methylation of primary and secondary amino groups (46) as described previously (35). [^{3}H]HCHO was used directly (98 mCi/mmol; PerkinElmer Life Sciences) or after dilution (10 Ci/mmol; ARC) with unlabeled HCHO. The reaction converted the ϵ-amino groups of two lysine residues (Lys^{16} and Lys^{28}) and the α-amino group of the N-terminal residue (Asp^1) to labeled dimethylamines (35), with specific activities of 400–1100 dpm/pmol of Aβ.

Preparation of Aβ Protofibrils—SEC-purified monomeric Aβ-(1–40) (100–140 μM) was incubated in 0.5–1 ml of 5–50 mM Tris-HCl, 5 mM EDTA (sodium salt), pH 8.0 (5–50 mM Tris-EDTA), at room temperature and agitated vigorously by continued vortexing to promote aggregation (35). Aggregation was monitored by thioflavin T fluorescence (35, 51), and the sample was microcentrifuged for 10 min in a tabletop centrifuge (Beckman Coulter) at 18,000 × *g*. The supernatant was chromatographed on a 1 × 30-cm Superdex 75 HR 10/30 column (Amersham Biosciences), and Aβ eluting in the void volume was defined as the protofibril fraction (35). Superdex columns were routinely pretreated with a bolus of BSA (50 mg) in running buffer to block nonspecific binding of Aβ protofibrils to the resin followed by a wash with at least 4 column volumes of running buffer. The columns also were occasionally washed with 1 N NaOH.

Circular Dichroism—Spectra were obtained on an Aviv model 215 circular dichroism spectrometer with a 0.1-cm path length quartz cuvette (Hellma) (41). Buffer control spectra were averaged and subtracted from the average of triplicate scans of each Aβ sample spectra, and each resulting point ($[\theta]_{obs}$, degrees) was converted to mean residue ellipticity ($[\theta]$, degrees cm^2 $dmol^{-1}$) with the equation, $[\theta] = [\theta]_{obs} \times (MRW/10lc)$, where MRW is the mean residue molecular weight of Aβ-(1–40) (4331 g/mol divided by 40 residues), l is the optical path length (cm), and c is the concentration (g/cm^3). Estimates of the predominant secondary structure were verified using the modified Contin method (CONTINLL) available through the CDPro suite of analysis programs with basis set 7 of the reference protein data base (47).

Dynamic Light Scattering (DLS)—Hydrodynamic radius (R_H) measurements were made at room temperature with a DynaPro MSX instrument (Protein Solutions Inc., Piscataway, NJ) equipped with a gallium aluminum arsenide laser. Samples (60 μl) were placed directly into a quartz cuvette, and total light scattering intensity at a 90° angle in kilocounts/s was collected using a 5-s acquisition time. Particle translational diffusion coefficients (D_T) were calculated from autocorrelated light intensity data (usually 20–25 points) and converted to R_H with the Stokes-Einstein equation ($R_H = k_bT/6\pi\eta D_T$). A histogram of percentage intensity *versus* R_H was calculated using Dynamics data analysis software (Protein Solutions), and intensity-weighted mean R_H values were obtained for each subpeak.

Multiangle Light Scattering (MALS)—Samples were applied to a Superdex 75 SEC column attached to an ÄKTA fast protein liquid

[2] Petkova, A. T., Leapman, R. D., Guo, Z., Yau, W. M., Mattson, M. P., and Tycko, R. (2004) *FASEB Meeting on Protein Misfolding, Amyloid and Conformational Disease*, poster abstract, Snowmass, CO (June 12–17).

chromatography system and analyzed in-line with a DAWN EOS MALS instrument (Wyatt Technology, Santa Barbara, CA) (35). Analysis of MALS data was based on the Zimm formalism of the Rayleigh-Debye-Gans model (48, 49), as presented previously (35). In brief, the excess Rayleigh ratio R_θ is related to the molecular structure according to Equation 1,

$$\frac{Kc}{R_\theta} = \frac{1}{MP(\theta)} + 2A_2c \qquad \text{(Eq. 1)}$$

where R_θ is proportional to the fraction of incident light that is scattered by the solute without interference; K is a physical constant equal to $4\pi^2(\mathrm{d}n/\mathrm{d}c)^2 n_o{}^2 N_A{}^{-1}\lambda_o{}^{-4}$, where n represents the refractive index of the solution, c is the solute concentration (g/ml), n_o is the refractive index of the solvent, N_A is Avagadro's number, and λ_o is the wavelength of the incident light in vacuum; A_2 is the second virial coefficient; and M is the molecular mass of the solute. At the low concentrations c employed in this study, the $2A_2c$ term in Equation 1 may be ignored. The function $P(\theta)$ is the ratio of the scattered light intensity to the scattered light intensity without interference. For larger molecules whose size approaches λ_o, the reciprocal $P^{-1}(\theta)$ may be expressed by the power series in Equation 2,

$$P^{-1}(\theta) = 1 + \frac{q^2 R_g{}^2}{3} + \ldots \qquad \text{(Eq. 2)}$$

where $q = (4\pi n_o/\lambda_o)\sin(\theta/2)$, θ is the angle between the incident and the scattered light, and R_g is the root mean square radius of gyration. According to Equations 1 and 2, a Zimm plot of Kc/R_θ as a polynomial in q^2 gives $(M)^{-1}$ as the y axis intercept and $R_g{}^2/3M$ as the limiting slope as θ approaches zero. When the solute is polydisperse, M and R_g become the weight-average molecular mass (M_w) and the z-average radius of gyration (R_{gz}), respectively. For very small molecules, $P(\theta)$ is equal to 1, and little slope is observed in the Kc/R_θ *versus* q^2 plot. This precludes R_{gz} determination but still allows M_w measurements if the concentration is known. Definitive concentration measurements from radioactivity allowed M_w determination of radiomethylated, monomeric Aβ-(1–40).

Electron Microscopy (EM)—Samples of Aβ aggregates were applied to 200-mesh Formvar-coated copper grids (Ernest F. Fullam, Inc., Latham, NY) and incubated for 10–15 min at room temperature. The sample was then wicked off with lens paper, washed briefly by placing the grid face down on a wash droplet, and stained by transferring the grid face down to a droplet of 2% uranyl acetate (Polysciences, Inc., Warrington, PA) for 5–10 min before wicking off the solution and air drying. With samples generated in 2% HFIP, all wash and treatment solutions applied to the grids also contained 2% HFIP. Grids were visualized in a Philips EM208S transmission electron microscope.

Atomic Force Microscopy (AFM)—Images were obtained as described previously (35). In brief, samples were applied to freshly cleaved mica that had been modified with 3′-aminopropyl-triethoxysilane and incubated for 15 min. The residual sample liquid was aspirated off, and the disk was then rinsed gently with water containing 2% HFIP and blown dry with compressed air. A Nanoscope III controller with a Multimode AFM (Digital Instruments, Santa Barbara, CA) was used for imaging by ambient tapping mode. Images here are presented in amplitude mode, where increasing brightness indicates greater damping of cantilever oscillation (34). Height mode images were "flattened" prior to the measurement of particle height distributions with NanoScope® III software (version 5.13r5; Digital Instruments).

RESULTS

Dissociation of Aβ Aggregates—Aggregates were prepared from unlabeled or radiomethylated Aβ-(1–40) monomer that had been purified by SEC (35). Radiomethylation of Aβ-(1–40) converts the primary amino groups on residues Asp[1], Lys[16], and Lys[28] to radiolabeled dimethylamines. This modification slows the assembly kinetics but does not affect the morphology of protofibrils or fibrils (35), and it significantly enhances the detection of Aβ. The monomeric nature of low molecular weight Aβ obtained from SEC was confirmed by multiangle light scattering in tandem with SEC. This analysis was conducted with radiomethylated Aβ for better quantitation and indicated a M_w of 4670 ± 90 (calculated M_W 4415 for the hexamethylated 1–40 peptide). The monomeric assignment was in agreement with translational diffusion measurements by NMR (50).

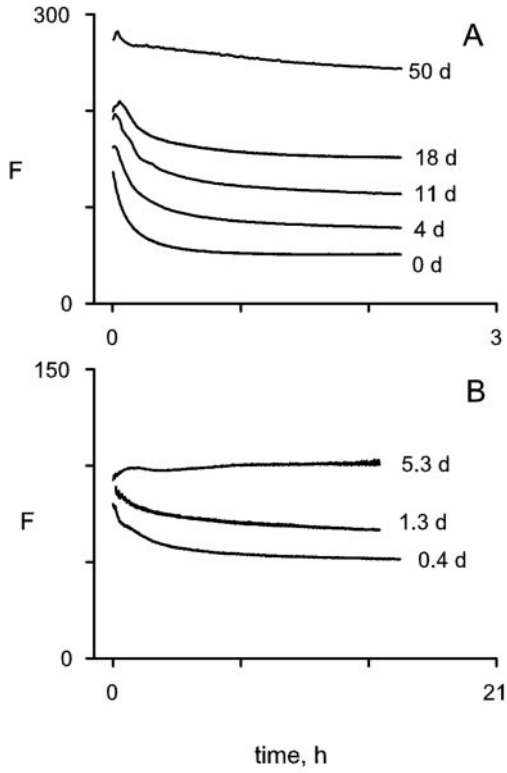

FIG. 1. **Aβ-(1–40) aggregates measured by thioflavin T fluorescence become more stable over time.** SEC-purified monomers of [^{3}H]Aβ-(1–40) (140 μM) in 50 mM Tris-EDTA (*A*) and unlabeled Aβ-(1–40) (100 μM) in 5 mM Tris-EDTA (*B*) were incubated with agitation for 22 h and maintained at room temperature without further manipulation. At the indicated times (in days), an aliquot was diluted 30-fold (*A*) or 40-fold (*B*) into 5 mM Tris-EDTA buffer containing 5 μM thioflavin T. The fluorescence (F) was fit to a five-parameter double exponential curve ($F = F_0 + ae^{-bt} + ce^{-dt}$) with SigmaPlot 8.0, where F_0 is the initial fluorescence, t is time, and b and d are fluorescence decay rate constants for fast and slow kinetic phases with amplitudes represented by a and c.

Monomeric Aβ-(1–40) was aggregated at low ionic strength with agitation as outlined previously (35), conditions that produced predominantly soluble protofibrils that could not be sedimented by centrifugation at 18,000 × *g*. After overnight aggregation, the reactions were incubated for various times before removing aliquots for large dilutions, which were necessary to minimize further monomer deposition and reveal disaggregation. The time course of disaggregation was conveniently monitored with thioflavin T, a fluorophore that shows greatly enhanced fluorescence on binding to amyloid fibrils (51). 30–40-fold dilution of Aβ-(1–40) aggregation reactions into buffer containing thioflavin T initiated a progressive decrease in fluorescence (Fig. 1). This decrease reflected disaggregation of the Aβ protofibrils, since it was accompanied by a decrease in DLS intensity and by an increase in the percentage of Aβ monomer as measured by SEC (see below). The fluorescence decrease occurred in at least two kinetic phases, with rapid initial disaggregation followed by a much slower secondary phase. For the earliest dilutions, the disaggregation rate constants for the rapid phase were 15 h^{-1} for the radiomethylated Aβ-(1–40) protofibrils (Fig. 1*A*) and 1 h^{-1} for the unlabeled protofibrils (Fig. 1*B*), indicating that the radiomethylated protofibrils were less stable than the unlabeled protofibrils. However, the most striking observation with both aggregation reactions was the progressive stabilization of the Aβ protofibrils, as demonstrated by decreased disaggregation rate constants and increased percentages of stable protofibrils after dilution at longer incubation times. For example, the percentage of initial

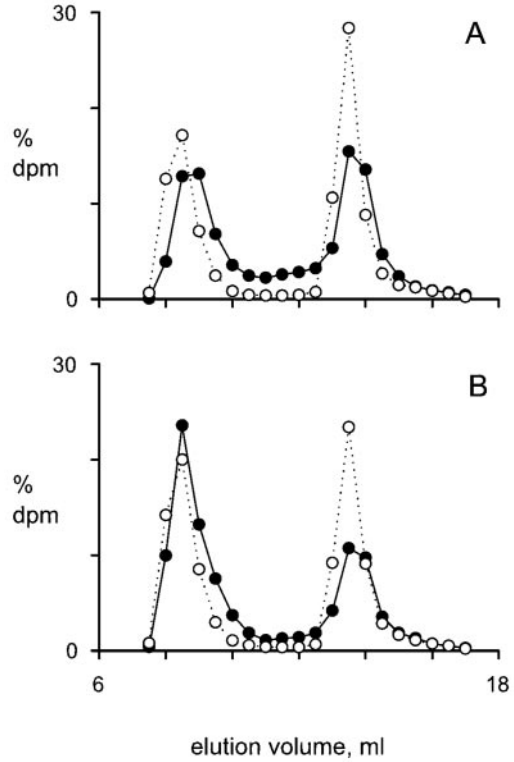

FIG. 2. **SEC analyses of an [^{3}H]Aβ-(1–40) aggregation reaction confirm monomer dissociation following dilution.** The aggregation reaction in Fig. 1*A* was incubated for 18 (*A*) and 42 days (*B*) and then fractionated by SEC in 5 mM Tris-EDTA. Samples were applied before (●, *solid line*) and 15 h after (○, *dotted line*) the dilution described in the legend to Fig. 1. Protofibril (7.5–12.5 ml) and monomer (13–17 ml) peaks were quantified by scintillation counting of collected fractions.

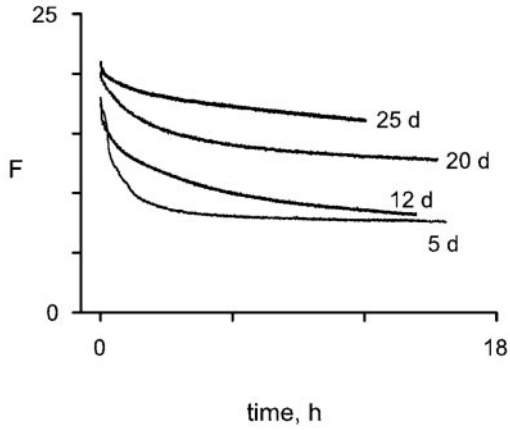

FIG. 3. **Isolated [^{3}H]Aβ-(1–40) protofibrils become more stable over time.** [^{3}H]Aβ-(1–40) protofibrils (12 μM), isolated by SEC in 5 mM Tris-EDTA, were incubated at room temperature for 1 month without further manipulation. Aliquots were diluted 16-fold into the same buffer at the indicated times, and protofibril content was measured by thioflavin T fluorescence as in Fig. 1.

fluorescence retained after disaggregation of the radiolabeled Aβ sample increased from 37% after dilution on the first day to 80% at 50 days (Fig. 1*A*).

To verify that the decrease in thioflavin T fluorescence in Fig. 1 corresponded to dissociation of Aβ monomers from protofibrils, the aggregation reactions before and after dilution were analyzed by SEC. However, analysis of the predilution radiomethylated protofibrils was complicated by apparent on-column dissociation during the SEC separation itself. This dissociation is illustrated by comparison of the radioactivity elution profiles for the pre- and postdilution 18-day samples in Fig. 2*A*. The predilution profile displayed radioactivity between the completely excluded protofibril peak (8–10 ml) and the monomer peak (13–15 ml). Experiments with larger samples have shown that the Aβ species in this region do not induce thioflavin T fluorescence, suggesting that they are monomers resulting from protofibril dissociation during the chromatography run rather than small oligomers (data not shown). Furthermore, this region of radioactivity vanished, and the monomer peak increased in the postdilution sample, clearly indicating that monomer dissociation had occurred. Quantitative comparison of the extent of dissociation with the fluorescence decrease in Fig. 1*A* was easier with the sample after stabilization during 42 days of incubation. SEC analysis showed that this sample, which produced much less radiolabel between the protofibril and monomer peaks (Fig. 2*B*), contained 32% monomer prior to dilution and 50% monomer 15 h after dilution. This 18% increase was in excellent agreement with the slow 20% decrease in fluorescence over this time period.

The shift in the compositions of the Aβ aggregation mixtures in Figs. 1 and 2 with increasing time of incubation reflected both continued monomer deposition and progressive stabilization of the protofibrils. Protofibrils prior to dilution of the radiomethylated sample in Fig. 1*A* increased from an initial 32% of total radiolabel to 68% after incubation for 42 days. One simple explanation for the stabilization is that smaller, less stable protofibrils rapidly disaggregate and disappear, whereas larger, more stable protofibrils continue to grow. However, size analysis of the samples in this experiment by DLS and MALS revealed little change in the R_H, R_{gz}, and M_w of the protofibrils during the 50-day incubation. Postdissociation protofibrils remaining after dilution had slightly larger R_{gz} values than the predilution protofibrils, suggesting that the loss of smaller, less stable Aβ aggregates makes a slight contribution to the overall stabilization.

Dissociation of Isolated Aβ Protofibrils—An unequivocal demonstration of the progressive stabilization of Aβ protofibrils was obscured in Figs. 1 and 2 by the presence of a significant concentration of Aβ monomer at all time points prior to dilution (for the [^{3}H]Aβ-(1–40), at least 40 μM). Continued deposition of monomer could simply have elongated the protofibrils without increasing the number of ends from which dissociation might occur, and this process would contribute to the apparent stabilization in Fig. 1. To eliminate this continued deposition from our analysis, we isolated freshly aggregated Aβ protofibrils by SEC prior to studying their dissociation on dilution. Some rapid monomer dissociation occurred during the isolation (see Fig. 2*A*), and considerable variability in stability was observed among different isolated protofibril preparations. Unlabeled Aβ-(1–40) protofibrils were more stable than radiomethylated Aβ-(1–40) protofibrils, as observed previously with the aggregation mixtures in Fig. 1, but even some radiomethylated protofibril preparations were extremely stable and did not show discernible monomer dissociation on dilution (data not shown). A less stable pool of isolated radiomethylated protofibrils was incubated at room temperature without perturbation, and aliquots were diluted into solutions with thioflavin T at various time points (Fig. 3). Fluorescence decreases again occurred in at least two kinetic phases, although the disaggregation rate constants for the initial phase were slower than those in Fig. 1 because some rapidly disaggregating species were lost during protofibril isolation. Significantly, a progressive time-dependent stabilization of the protofibrils was observed even in the absence of monomer (Fig. 3). Disaggregation rate constants decreased, and higher percentages of stable

protofibrils remained after dilution as the protofibrils aged. Here the increase in protofibril stability was accompanied by a gradual increase in average protofibril R_H from 50 nm immediately after isolation to 98 nm after 26 days. We have shown previously that this increase in average R_H in the absence of monomer results from association of protofibrils to form larger protofibrils and fibrils (35). Mechanisms contributing to the progressive stabilization of isolated protofibrils in the absence of monomer deposition remain to be identified but may include protofibril association.

Dilute HFIP Promotes Rapid Formation of Unstable Aβ Aggregates—The data we have presented so far indicate that Aβ-(1–40) protofibrils become progressively more stable with continued incubation. We now show that Aβ aggregates are formed rapidly in dilute HFIP, and these aggregates exhibit a dramatically broader range of stability. HFIP is widely known as an effective solvent for Aβ peptides (52). Aβ-(1–40) protofibrils and fibrils were solubilized at HFIP concentrations above 20% (v/v), as indicated by loss of thioflavin T fluorescence and conversion to monomeric Aβ on SEC (data not shown). However, low concentrations of HFIP were striking in their ability to promote Aβ aggregation. The time scale for nonagitated aggregation of Aβ-(1–40) was reduced from weeks to minutes over a narrow range of HFIP concentrations from 1 to 2% (v/v) (see Fig. 4*A*), and the usual lag time for Aβ aggregation (35, 53) was abolished. Most of the Aβ appeared to aggregate in 2% HFIP, since the maximum thioflavin T fluorescence per μM total Aβ was comparable for the protofibrils in Fig. 1 and the HFIP-induced aggregates in Fig. 4*A*. However, slightly less aggregation was observed at 4% HFIP, and none was observed at 10% HFIP. The aggregation did not require a particular mixing sequence, since similar rates were observed when stock Aβ in 50% HFIP was diluted or a small volume of neat HFIP was added to diluted Aβ (data not shown). The HFIP induced aggregates were soluble, since virtually no fluorescence was removed from the supernatant after centrifugation of the reactions in Fig. 4*A* at 18,000 × *g* for 10 min. Although radiomethylation slows the aggregation of Aβ-(1–40) (35) and Aβ-(1–42) (data not shown) by roughly an order of magnitude in our routine Aβ aggregation procedure (as defined in Fig. 1), this effect is lost in 2% HFIP, since unlabeled and radiomethylated Aβ-(1–40) aggregated at similar rates (Fig. 4*B*). Aβ-(1–42) *in vitro* is more prone to aggregation into protofibrils and fibrils than Aβ-(1–40) (31, 32), and this difference is retained in 2% HFIP even after radiomethylation of Aβ-(1–42) (Fig. 4*B*).

Dilution of HFIP into aqueous buffers gives a dispersion with modest DLS intensity, probably resulting from the formation of a polydisperse population of HFIP microdroplets, discussed with Fig. 7, below. These microdroplets represented only a tiny fraction of the dissolved HFIP, since most of the HFIP particles responsible for the light scattering intensity were removed by centrifugation at 18,000 × *g* for 10 min with less than a 5% decrease in the supernatant HFIP concentration as measured by ^{19}F NMR (data not shown). However, the rate of Aβ-(1–40) aggregation was significantly slowed in these HFIP supernatants relative to that in the initial HFIP dispersion (Fig. 4*C*). Ultracentrifugation of the HFIP supernatant at 100,000 × *g* for 1 h had no further effect on either light scattering intensity or the Aβ-(1–40) aggregation rate. The light scattering components initially in dilute HFIP also could be eliminated simply by storing the solution for several days, and this storage (or "aging") also was sufficient to slow the Aβ-(1–40) aggregation rate (Fig. 4*C*).

The Aβ aggregates formed in dilute HFIP appeared to possess significant β-structure based on their fluorescence with thioflavin T. This structure was confirmed by CD analysis

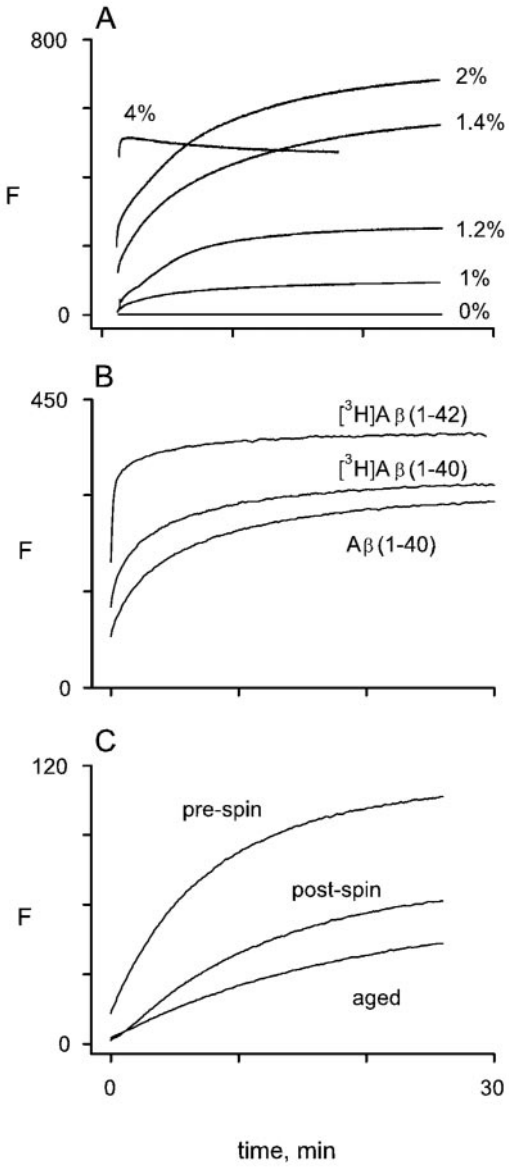

FIG. 4. **Low concentrations of HFIP dramatically accelerate the aggregation of Aβ peptides.** *A*, undiluted HFIP was added to the indicated final percentages (v/v) to solutions containing SEC-purified monomeric Aβ-(1–40) (20 μM) and 5 μM thioflavin T in 30 mM Tris-HCl (pH 8.0), and continuous fluorescence measurements were initiated immediately. *B*, the aggregations of SEC-purified unlabeled and radiomethylated Aβ monomers (10 μM) in 5 mM Tris-EDTA containing 2% HFIP. *C*, a 4% HFIP solution in water (*pre-spin*) was centrifuged at 18,000 × *g* for 10 min (*post-spin*) or sealed and stored for 8 days (*aged*). Light scattering intensity by DLS decreased from 428 kilocounts/s before to 17 kilocounts/s after centrifugation. Aliquots were mixed with an equal volume of SEC-purified monomeric [^{3}H]Aβ-(1–40) (20 μM) in 60 mM Tris-EDTA.

below. Therefore, it was surprising that the aggregates initially were very unstable when diluted into buffer and thioflavin T without HFIP (Fig. 5A). 15-fold dilution of the aggregates formed after 30 min in 2% HFIP resulted in a fluorescence decrease so fast that actual measurement was precluded. In contrast, maintenance of the HFIP at 2% in the dilution buffer significantly slowed the fluorescence decrease (Fig. 5*A*). It appears that HFIP at low concentrations is a significant stabilizing agent for Aβ aggregates that were initially formed in dilute HFIP.

Prolonged incubation of Aβ-(1–40) in dilute HFIP resulted in a marked stabilization of the aggregates without an increase in the overall thioflavin T binding (Fig. 5*B*). Disaggregation rate

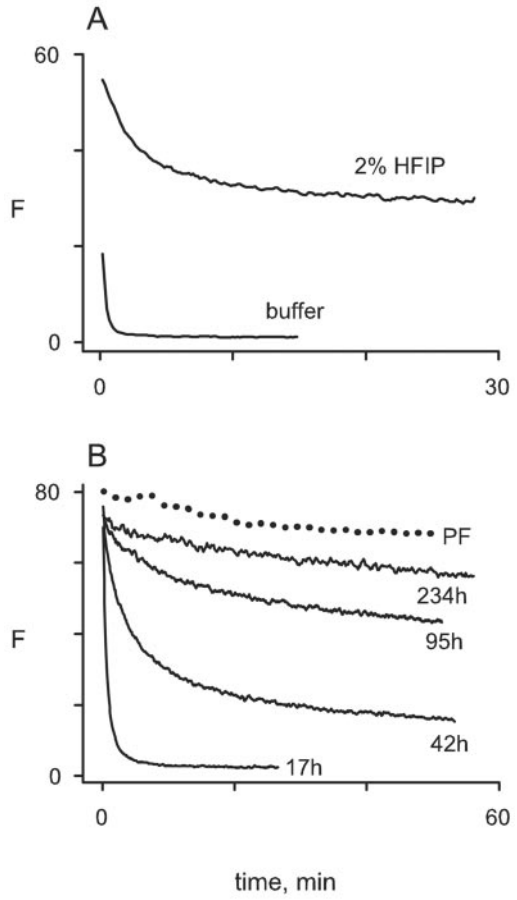

FIG. 5. **Aβ-(1–40) aggregates induced by dilute HFIP initially are very unstable but stabilize over time.** *A*, SEC-purified monomeric Aβ-(1–40) (20 μM) was incubated without agitation in 5 mM Tris-EDTA containing 5 μM thioflavin T and 2% (v/v) HFIP for 30 min at room temperature. A rapid increase in fluorescence similar to that in Fig. 4 was observed. Disaggregation was then initiated by diluting the mixture 15-fold into the same buffer with thioflavin T with or without 2% HFIP, and the decrease in fluorescence was monitored. *B*, conditions were identical to those in *A* except that the 2% HFIP aggregation was buffered with 50 mM Tris-EDTA and Aβ-(1–40) was 60 μM, and 15-fold dilutions were made at the indicated times. The 0.4-day disaggregation curve from Fig. 1*B* (*dotted line*) is reproduced in *B* to allow comparison with Aβ-(1–40) protofibrils.

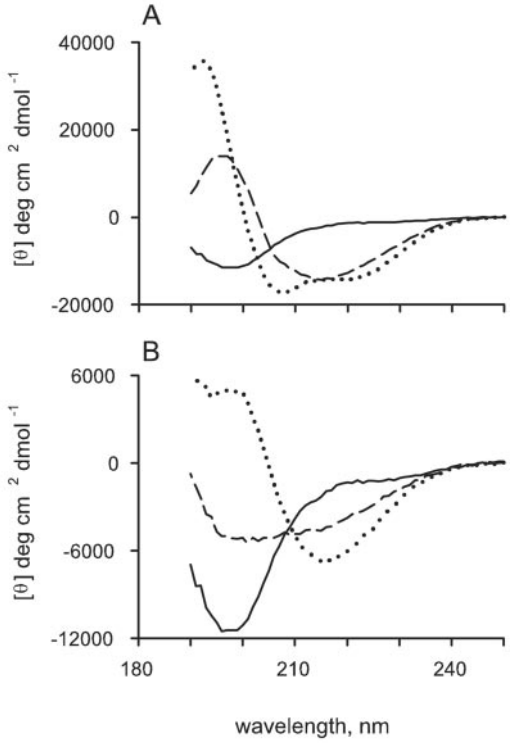

FIG. 6. **Circular dichroism spectra for monomeric and aggregated Aβ.** *A*, Aβ-(1–40) (30 μM) in three conformational states. Shown are spectra for stock monomeric Aβ-(1–40) in 5 mM Tris-HCl (pH 8.0) (*solid line*) or after the addition of 30% HFIP (*dotted line*). Aβ-(1–40) protofibrils were isolated by SEC in the same buffer (*dashed line*). The protofibril concentration (in Aβ monomer units) was estimated from absorbance corrected for light scattering (35) and confirmed by absorbance ($\epsilon_{276\ nm}$ of 1450 $cm^{-1}\ M^{-1}$) following dissolution by the addition of HFIP to 30%. *B*, CD spectra for monomeric Aβ-(1–40) (30 μM) in 5 mM Tris-HCl (*solid*) and after incubation for 24 h with 2% HFIP. The HFIP was added either neat (*dotted line*) or from 4% HFIP in water that had been aged for 1 month and centrifuged at 18,000 × *g* for 10 min (*dashed line*). The *solid line* from *A* is shown for comparison.

constants on dilution into buffer without HFIP were decreased and, after nearly 10 days, approached the rate constant obtained for disaggregation of Aβ protofibrils formed in the absence of HFIP. The HFIP-induced aggregates remained soluble despite this stabilization. In only one case, after incubation in 2% HFIP for several days at a higher buffer concentration (30 mM Tris-HCl), were the aggregates sedimented at 18,000 × *g* for 10 min. Although similar initial disaggregation rates were observed for radiomethylated and unlabeled Aβ-(1–40) aggregates produced in 2% HFIP, the radiolabeled aggregates showed much less stabilization over time.

Both Aβ Protofibrils and HFIP-induced Aβ Aggregates Are Rich in β-Structure—Previous analyses of CD spectra for 39–42-residue Aβ peptides prior to aggregation have concluded that the conformations are largely random coil in aqueous buffers (37, 54) and predominantly α-helical in acidic (55) and neutral (56) pH solutions that contain ≥20% HFIP. Our spectra in Fig. 6*A* are consistent with these conclusions, as indicated by the presence of a single minimum at 197 nm for stock monomeric Aβ-(1–40) in buffer and double minima at 208 and 222 nm for the stock Aβ-(1–40) in buffer with 30% HFIP. In contrast, Aβ-(1–40) protofibrils isolated by SEC exhibit a minimum at 216 nm and a maximum at 195 nm (Fig. 6*A*), indicating a preponderance of β-structure (sheet and turn) as reported previously for Aβ-(1–40) fibrils (57) and protofibrils (58) generated *in vitro*. The addition of monomeric Aβ-(1–40) to fresh 2% HFIP gave a rapid increase in thioflavin T fluorescence in Fig. 4*A*, suggesting formation of an amyloid aggregate rich in β-structure, and this was supported by the minimum at 216 nm in the CD spectra in Fig. 6*B*. The addition of monomeric Aβ-(1–40) to 2% HFIP that had been centrifuged to remove apparent HFIP aggregates gave a smaller increase in thioflavin T fluorescence in Fig. 4*C*, and this correlated with a smaller shift at 216 nm in the corresponding CD spectrum in Fig. 6*B*. Inclusion of the random coil spectrum for control monomeric Aβ-(1–40) in Fig. 6*B* revealed an isodichroic point at 209 nm for these three solutions, indicating a two-component mixture with varying amounts of the component rich in β-structure. Given the instability of this component on dilution in Fig. 5*A*, we infer that the mixture involved a rapid equilibrium between the random coil and β-structures. Our data are consistent with a previous report that Aβ-(1–40) formed β-structure at HFIP concentrations of 3–10% (56).

HFIP-induced Aβ Aggregates Initially Are Globular but Progress to Fibers—DLS and MALS are effective tools for structural analysis of large but still soluble particles, and both have been used previously to characterize Aβ protofibrils (32, 35). Like protofibrils, the HFIP-induced Aβ aggregates generally were soluble following centrifugation at 18,000 × *g* for 10 min. R_H values obtained by DLS for the initial Aβ aggregates in-

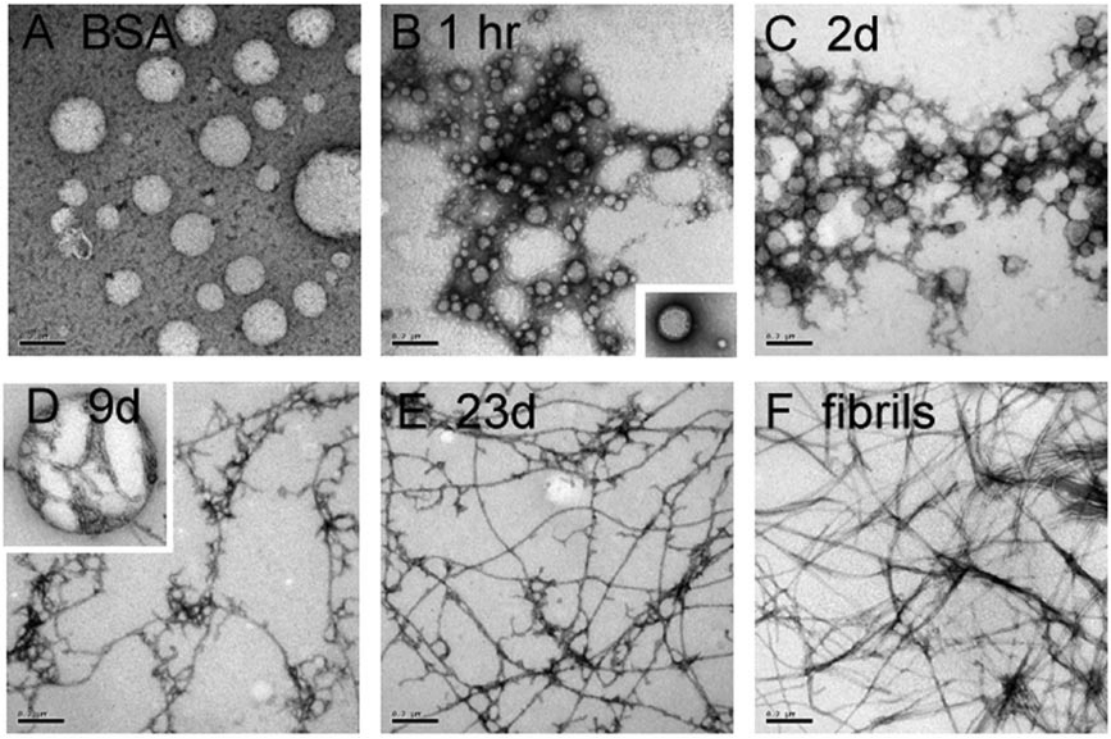

FIG. 7. **Electron micrographs of HFIP-induced Aβ-(1–40) aggregates reveal progressive changes in morphology.** Bovine serum albumin (0.25 mg/ml) (*A*) or SEC-purified monomeric Aβ-(1–40) (40 μM) (*B–E*) were incubated in 5 μM thioflavin T, 5 mM Tris-HCl (pH 8.0), and 2% HFIP (undiluted) at room temperature. After 0.1 h, a 10-μl sample of the BSA solution was removed, and at the indicated times, aliquots of the Aβ-(1–40) solution were centrifuged at 18,000 × *g* for 10 min and supernatant samples (10 μl) were removed. These samples were processed for negative staining and EM. *F*, SEC-purified monomeric Aβ-(1–40) (100 μM) in 30 mM Tris-Cl (pH 8.0) was incubated with agitation for 22 h. An aliquot was centrifuged (18,000 × *g* for 10 min) and diluted 30-fold, and the protofibrils in the supernatant were elongated by the addition of monomeric Aβ-(1–40) (30 μM) for 15 min. A 10-μl sample was removed for negative staining and EM as in *A–E*. *Images* and *insets* are shown relative to a *calibration bar* of 200 nm.

duced in 2% HFIP ranged from 30 to 80 nm, similar to those obtained previously for Aβ-(1–40) protofibrils (35), but a second subpeak with $R_H > 300$ nm emerged after several days in 2% HFIP. Analysis of the HFIP-induced Aβ aggregates by SEC separation in-line with MALS (SEC-MALS) was complicated by their rapid disaggregation, but measurements were obtained when the aggregates were stabilized by inclusion of 2% HFIP during SEC. Zimm plots indicated that the M_w of the HFIP-induced aggregates of radiomethylated Aβ ranged from 18 to 25×10^3 kDa and that their *z*-average radius of gyration (R_{gz}) ranged from 90 to 110 nm. These values also are comparable with those we measured previously for radiomethylated Aβ-(1–40) protofibrils (35).

To determine whether the progressive stabilization of HFIP-induced Aβ aggregates that occurred during continued incubation of the aggregation reactions was accompanied by morphological changes, we examined the aggregation reactions by EM and AFM. EM analysis was conducted following negative staining of samples with uranyl acetate. Control samples of freshly diluted 2% HFIP showed no features in EM images, but the addition of BSA to the diluted HFIP resulted in the appearance of circular objects (Fig. 7*A*). The number of these objects was greatly reduced when the 2% HFIP solutions were centrifuged at 18,000 × *g* for 10 min before and after the addition of BSA (data not shown). These observations implied that BSA had slightly adsorbed to spherical HFIP aggregates and supported the evidence from DLS above that HFIP forms a dispersion of microdroplets in dilute aqueous solution. A solution of Aβ-(1–40) was prepared in freshly diluted 2% HFIP, and aliquots were removed at several time points, centrifuged at 18,000 × *g* for 10 min, and examined by EM. After 1 h of incubation, clustered globular structures were the predominant negatively stained feature (Fig. 7*B*). Some individual globular structures also were observed (Fig. 7*B*, *inset*). The diameter of the globules extended over a range of 20–200 nm, and punctate deposits could be seen on several of the larger globules. The globules presumably represented HFIP microdroplets upon which Aβ had deposited and begun to aggregate. However, based on their fluorescence with thioflavin T, these Aβ deposits differed from the BSA-coated microdroplets by remaining soluble after centrifugation at 18,000 × *g*. Two days later, the clustered globular structures were incorporated into a mesh or lattice of fiber-like elements (Fig. 7*C*), and after 9 days, more distinct fibers were apparent (Fig. 7*D*). These included long fibers from which many short fibers branched and, very rarely, structures resem-

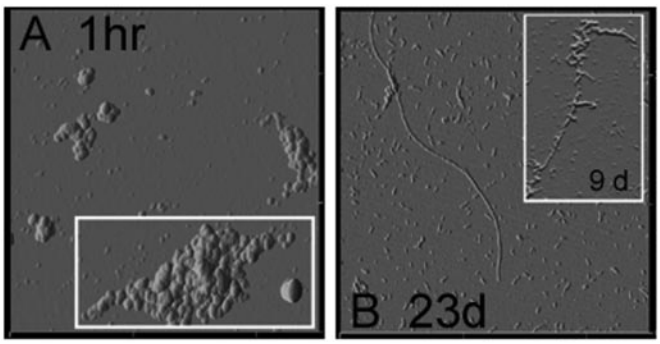

FIG. 8. **AFM images of HFIP-induced Aβ-(1–40) aggregates also show changes in morphology with time.** Samples were taken at the indicated times from the same incubated solution of Aβ-(1–40) in 2% HFIP described in Fig. 7 and diluted 25-fold with 2% HFIP. Aliquots (100 μl) were applied directly to the mica surface. *Images* are 2.5 × 2.5 μM, and *insets* are on this same scale.

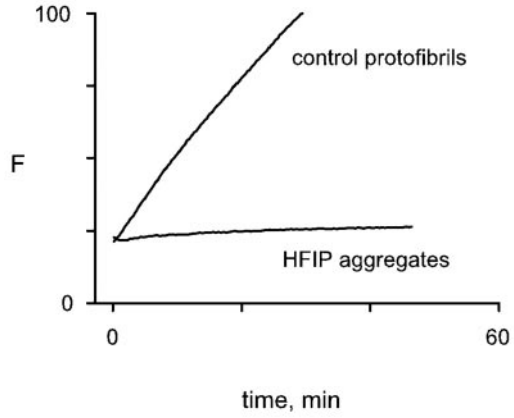

FIG. 9. **Aβ-(1–40) aggregates induced by dilute HFIP do not elongate as efficiently as Aβ-(1–40) protofibrils.** Aβ-(1–40) aggregation (50 μM) was induced in 2% (v/v) HFIP as in Fig. 4*B* and incubated for 3 days to promote stabilization. The solution was centrifuged at 18,000 × *g* for 10 min, and the Aβ aggregates in the supernatant were diluted 5-fold in the same buffer for 1 h and then mixed with an equal volume of 5 mM Tris-EDTA and 5 μM thioflavin T with or without Aβ-(1–40) monomer (60 μM final concentration). Fluorescence traces for these samples were recorded, and the difference in these traces was added to the initial fluorescence to give the *solid curve* labeled HFIP. Elongation of control protofibrils (diluted to 1 μM, which matched the initial HFIP aggregate fluorescence) with monomer (60 μM) was conducted in parallel. R_H values for protofibrils and HFIP-induced aggregates prior to elongation were 205 and 196 nm, respectively.

bling initial microdroplets on which fibers had formed (Fig. 7*D*, *inset*). After 23 days (Fig. 7*E*) the HFIP-induced fibers appeared similar to control fibrils produced by elongation of Aβ-(1–40) protofibrils (Fig. 7*F*), but numerous short branches remained that were not found on the control fibrils.

AFM images supported and extended the features of HFIP-induced Aβ aggregates observed by EM. The same mixture of clustered globular structures and individual globules was observed 1 h after adding Aβ-(1–40) to dilute HFIP (Fig. 8, *A* and *inset*). The heights of the clustered structures typically ranged from 10 to 15 nm but in some cases extended to over 50 nm. After 23 days, fibers with heights of 4–5 nm had appeared, and numerous very short rods with heights of 2.5–4 nm had emerged that were barely evident in the 1-h sample (Fig. 8*B*). These short rods were less clear in the EM images, perhaps because of differences in retention on the EM grid and AFM mica surfaces or because they showed little negative staining. A 9-day image showed a fiber-like structure with several branching arms (Fig. 8*B*, *inset*), consistent with the branched fibers observed by EM.

HFIP-induced Aβ Aggregates Elongate More Slowly than Aβ Protofibrils—The HFIP-induced Aβ aggregates approached the stability of Aβ-(1–40) protofibrils after incubation for 10 days (Fig. 5*B*) To examine whether stabilization resulted in some structural convergence of these two species, we determined their relative rates of elongation in the presence of added Aβ-(1–40) monomer (Fig. 9). The HFIP-induced Aβ aggregates were diluted in two steps, first to eliminate less stable aggregates and lower the HFIP concentration and then to introduce monomer. The fluorescence signal still showed slight disaggregation even with monomer, but the rate of disaggregation was clearly slower than that observed following a control dilution into solution that did not contain Aβ monomer (data not shown). Therefore, the net elongation rate of the HFIP-induced Aβ aggregates was very small compared with that of Aβ-(1–40) protofibrils (Fig. 9), with the latter rate being almost 30 times faster than the former. The difference in elongation rates was not due to a difference in aggregate sizes or concentrations, since the R_H values were similar (Fig. 9) and the aggregate concentrations were matched to the same initial thioflavin T fluorescence. We concluded that the seeding efficiency of the HFIP-induced aggregates was much lower than that of protofibrils in aqueous buffers without HFIP.

DISCUSSION

Several examples of polymorphism of soluble Aβ-(1–40) aggregates are highlighted in this report. All of the aggregates exhibited some of the classic features of amyloid structures, including the binding of thioflavin T with enhancement of its fluorescence and a predominance of β-structure as measured by CD. However, they differed in morphology, in the capacity to seed Aβ-(1–40) monomer deposition, and most strikingly in stability. Differences in stability arose not only from alternative aggregation conditions but also from progressive changes in the aggregates once they were formed. Progressive changes in the morphology of small Aβ aggregates (59) and Aβ fibrils (60) have been observed previously, but the stability of Aβ aggregates has received much less attention. Virtually the only quantitative estimate of an *in vitro* disaggregation rate for soluble Aβ aggregates involved Aβ-(1–40) protofibrils trace-labeled with [^{125}I]Aβ-(1–40). The dialyzed protofibrils released only about 30% of their radioactivity, mostly over the first 2 days of dialysis (58). This observation is quite compatible with the extent of disaggregation of Aβ-(1–40) protofibrils that we observed in Fig. 1*B*.

The Dock and Lock Model of Aβ Fibril Elongation—Two additional reports have focused on the dissociation of Aβ after fresh deposition of Aβ monomer on a solid phase Aβ fibril template. In an elegant study by Maggio and co-workers (61), radioiodinated Aβ-(1–40) monomer was deposited onto immobilized synthetic Aβ-(1–40) fibrils for varying periods of time, and release of ^{125}I-labeled monomers from the washed fibrils was then monitored. The dissociation kinetics expected in this experiment depend on the amount of radiolabeled monomer deposited. If deposition occurred only at a uniform population of growth points (*e.g.* fibril ends), deposited Aβ would dissociate with simple first order kinetics when the number of ends exceeded deposited Aβ and with zero-order kinetics when the number of ends was much smaller than deposited Aβ. Dissociation would follow an exponential time course in the first case and a linear time course in the second, and this linear rate would be the same regardless of the amount of deposited Aβ. The data revealed a more complicated process, with a rapid dissociation phase followed by slower phase(s) indicating that the growth points are not homogeneous. Furthermore, the percentage of deposited monomer that rapidly dissociated was found to depend on the length of time the monomer was in contact with the growing fibril. More than 80% of the radiolabel dissociated within 2 h after deposition times of 30 min or less, whereas less than 30% dissociated within 3 days after 12 h of deposition. The authors proposed a "dock and lock" model in which Aβ monomer deposits (docks) onto the growing fibril and then slowly converts (locks) to a conformation that dissociates from fibril ends much more slowly. These fast and slow components were resolved by a double-exponential dissociation equation, but such an analysis should be applied with caution. If much of the dissociation actually involved a constant linear dissociation rate as noted above, a double exponential analysis would appear to show an increase in the slow component at longer deposition times when more monomer was deposited. This concern was addressed in the second report, where fibrillar Aβ-(1–40) was covalently linked to Biacore biosensor chips and the deposition and subsequent dissociation of monomeric Aβ-(1–40) was monitored by surface plasmon resonance (62, 63). Dissociation was again characterized by fast and slow phases, but in Ref. 62, the total deposited monomer was held

constant by varying the free monomer concentration over different exposure times. Progressive stabilization was apparent, as the amplitude of the fast dissociation phase became smaller after longer exposure times, and the dock and lock model was invoked to explain this phenomenon (62).

While the dock and lock model can explain some of the protofibril stabilization observed in Fig. 1, it may be too limiting. Over 50% of the protofibril fluorescence is lost following the initial dilution in Fig. 1*A*, despite the fact that the size of the protofibrils obtained with our aggregation and SEC isolation procedures exceeds 1500 monomer units (see Ref. 35). Furthermore, the isolated Aβ protofibrils underwent progressive stabilization even in the absence of monomer. These observations suggest that protofibrils become more stable not just at their ends but through an intrinsic secondary or tertiary structural change extending over a substantial portion of the protofibril (*e.g.* tightening of the amyloid filament β-sheet structure).

A Critical Monomer Concentration for Aβ Aggregation—The progressive stabilization of Aβ protofibrils that we observed in Fig. 1 raises concerns about estimates by some groups of a critical monomer concentration, M_C, required for *in vitro* Aβ aggregation. Estimates of M_C for Aβ-(1–40), based on the soluble Aβ remaining after 3–5 days of incubation in buffered saline at pH 7.4, ranged from 6 to 35 μM (64) (see Ref. 65). The equilibrium assumed in M_C determinations is very difficult to achieve if the rate constants for monomer addition to protofibril ends (k_{on}) and monomer dissociation from these ends (k_{off}) are continually decreasing. When aggregated Aβ is at equilibrium with Aβ monomer, $M_C = k_{off}/k_{on}$ (66, 67). Aggregate growth by monomer deposition occurs when monomer concentrations are greater than M_C, and M_C estimates by this criterion are considerably smaller than those obtained from solubility determinations. Elongation of fibrillar Aβ-(1–40) on biosensor surfaces occurred at Aβ-(1–40) monomer concentrations as low as 0.2 μM, and estimates of M_C were about 0.02 μM (63). Solution measurements of protofibril growth by elongation with thioflavin T (as in Fig. 9) have less sensitivity than the biosensor, but we have detected monomer deposition and net growth at Aβ-(1–40) monomer concentrations of 0.5 μM.[3] We suggest that the difference between solubility and kinetic estimates of M_C arises because these structures not only become more resistant to disaggregation with time but also become more resistant to elongation.

Dilute HFIP Appears to Promote Interfacial Aβ Aggregation—The rapid formation of unstable Aβ aggregates in 1–2% HFIP is a striking illustration of Aβ aggregate polymorphism. All of the features of dilute aqueous solutions of HFIP that promote the formation of these aggregates are not yet defined, but we propose that they include Aβ interactions at interfaces generated by the formation of HFIP microdroplets in the aqueous solvent. This proposal is consistent with our observation of BSA-coated spherical aggregates of HFIP in the EM images in Fig. 7*A* and with the demonstration in Fig. 4*C* that centrifugation of the 2–4% HFIP stocks removed light scattering particles and decreased the rate and extent of Aβ aggregation. Aβ is an amphipathic molecule, and we have recently reported a dramatic acceleration of Aβ aggregation at the interface of a macroscopic two-phase system formed by buffer and chloroform (41). These two-phase Aβ aggregates, like those induced in dilute HFIP, contained primarily β-structure according to their CD spectra and rapidly disaggregated upon dilution. The two-phase Aβ aggregates also formed globular species that progressed to fibers based on AFM images, but these globular structures were smaller and more uniform than those initially formed in dilute HFIP. Previously reported biophysical analyses of aqueous HFIP solutions also support a microdroplet structure. NMR and small angle neutron scattering data have indicated microheterogeneities that are maximized at HFIP concentrations of about 35% (v/v), with clusters involving hydrophobic CF_3 groups aggregated in an inside core and hydrophilic OH groups forming hydrogen bonds with surrounding water molecules (68). Below these concentrations, mass spectrometry revealed hydrated HFIP oligomers of stoichiometry $(HFIP)_m(H_2O)_n$. At 2–4% HFIP (v/v), oligomers with $m = 2–4$ and $n = 5–20$ were detected, but larger oligomers were not explored because of the limited mass number range employed (68).

The process by which the initial Aβ aggregates formed on HFIP microdroplet clusters convert to fibers is unclear. Because of the initial instability of these HFIP-induced aggregates, the growth of fibers may reflect monomer dissociation from the globular clusters and redeposition on more stable nascent fibers. However, the rare cases of relatively well formed fibers on spherical structures that resemble microdroplets (Fig. 7*D*, *inset*) suggest that some reorganization of the initial β-structured aggregates can occur directly on the microdroplet surface.

Despite the differences between Aβ protofibrils and HFIP-induced aggregates, they both showed progressive stabilization after initial aggregate formation. After several days of stabilization, the HFIP-induced aggregates formed fibers that had some resemblance to elongated protofibrils (Fig. 7). However, these aggregates still seeded monomer elongation with very different efficiencies (Fig. 9). Further studies are required to determine the molecular interactions in these aggregates, but models of amyloid fibrils suggest ways in which differences could arise. In the structural model for Aβ-(1–40) based on solid-state NMR data, a cross-β unit is composed of two β-strand segments involving residues 12–24 and 30–40 separated by a segment with a bend angle of 180°, allowing interpeptide hydrogen bonding and separate parallel β-sheet formation from both β-strands (24). In contrast, low angle x-ray diffraction analysis of Aβ-(11–25) fibrils indicated an antiparallel alignment of fully extended β-strands (69). In these fibrils, the β-sheets appeared to stack by slipping relative to each other by the length of two amino acid units (69), and the registry of the hydrogen bonding appeared to vary with pH (24). It is possible then that Aβ-(1–40) protofibrils and HFIP-induced aggregates differ by their β-strand alignments or the registry of their β-sheets or hydrogen bonding, and solid state NMR measurements will be required to resolve this issue.

It will be of interest to determine whether agents or conditions that favor rapid interfacial formation of unstable Aβ aggregates occur *in vivo*. Analogs of biological membranes, namely G_{M1} ganglioside micelles and artificial lipid rafts that contain G_{M1} (40), as well as lipoprotein particles (70) have been reported to bind Aβ peptides in a saturable manner and to convert the peptide conformations to β-structures in the complexes. The stability of these aggregates has not been investigated. A recent study also has found that inhaled anesthetics promote Aβ aggregation (30). The haloalkane halothane and the haloether isoflurane, like HFIP, are highly fluorinated, and both increased the rates of Aβ aggregation as measured by thioflavin T fluorescence. Furthermore, an EM image of the Aβ aggregates induced by halothane at concentrations achieved in routine clinical anesthesia (<1 mM) was strikingly similar to those in Fig. 7, *C* and *D*, here. The authors suggested that cytotoxicity induced by these aggregates may contribute to persistent postoperative cognitive problems that occur in the elderly.

[3] M. R. Nichols, M. A. Moss, D. K. Reed, and T. L. Rosenberry, unpublished observations.

Acknowledgment—We thank Dr. Wen-Lang Lin (Mayo Clinic, Jacksonville, FL) for the suggestion that we explore the interaction of control proteins like BSA with putative HFIP microdroplets by EM.

REFERENCES

1. Cohen, A. S., and Calkins, E. (1959) *Nature* **183,** 1202–1203
2. Glenner, G. G., and Wong, C. W. (1984) *Biochem. Biophys. Res. Commun.* **120,** 885–890
3. Miller, D. L., Papayannopoulos, I. A., Styles, J., Bobin, S. A., Lin, Y. Y., Biemann, K., and Iqbal, K. (1993) *Arch. Biochem. Biophys.* **301,** 41–52
4. Selkoe, D. J. (2001) *Physiol. Rev.* **81,** 741–766
5. Hardy, J. A., and Higgins, G. A. (1992) *Science* **256,** 184–185
6. Selkoe, D. J., and Podlisny, M. B. (2002) *Annu. Rev. Genomics Hum. Genet.* **3,** 67–99
7. Nilsberth, C., Westlind-Danielsson, A., Eckman, C. B., Condron, M. M., Axelman, K., Forsell, C., Stenh, C., Luthman, J., Teplow, D. B., Younkin, S. G., Naslund, J., and Lannfelt, L. (2001) *Nat. Neurosci.* **4,** 887–893
8. Yankner, B. A. (1996) *Nat. Med.* 850–852
9. Hardy, J., and Selkoe, D. J. (2002) *Science* **297,** 353–356
10. Hartley, D. M., Walsh, D. M., Ye, C. P., Diehl, T., Vasquez, S., Vassilev, P. M., Teplow, D. B., and Selkoe, D. J. (1999) *J. Neurosci.* **19,** 8876–8884
11. Klein, W. L., Krafft, G. A., and Finch, C. E. (2001) *Trends Neurosci.* **24,** 219–224
12. Westerman, M. A., Cooper-Blacketer, D., Mariash, A., Kotilinek, L., Kawarabayashi, T., Younkin, L. H., Carlson, G. A., Younkin, S. G., and Ashe, K. H. (2002) *J. Neurosci.* **22,** 1858–1867
13. Kawarabayashi, T., Shoji, M., Younkin, L. H., Lin, W. L., Dickson, D. W., Murakami, T., Matsubara, E., Abe, K., Ashe, K. H., and Younkin, S. G. (2004) *J. Neurosci.* **24,** 3801–3809
14. Lambert, M. P., Barlow, A. K., Chromy, B. A., Edwards, C., Freed, R., Liosatos, M., Morgan, T. E., Rozovsky, I., Trommer, B., Viola, K. L., Wals, P., Zhang, C., Finch, C. E., Drafft, G. A., and Klein, W. L. (1998) *Proc. Natl. Acad. Sci. U. S. A.* **95,** 6448–6453
15. Walsh, D. M., Klyubin, I., Fadeeva, J. V., Cullen, W. K., Anwyl, R., Wolfe, M. S., Rowan, M. J., and Selkoe, D. J. (2002) *Nature* **416,** 535–539
16. Hsia, A., Masliah, E., McConlogue, L., Yu, G., Tatsuno, G., Hu, K., Kholodenko, D., Malenka, R. C., Nicoll, R. A., and Mucke, L. (1999) *Proc. Natl. Acad. Sci. U. S. A.* **96,** 3228–3233
17. Sunde, M., Serpell, L. C., Bartlam, M., Fraser, P. E., Pepys, M. B., and Blake, C. C. (1997) *J. Mol. Biol.* **273,** 729–739
18. Serpell, L. C., Sunde, M., Benson, M. D., Tennent, G. A., Pepys, M. B., and Fraser, P. E. (2000) *J. Mol. Biol.* **300,** 1033–1039
19. O'Nuallain, B., and Wetzel, R. (2002) *Proc. Natl. Acad. Sci. U. S. A.* **99,** 1485–1490
20. Kayed, R., Head, E., Thompson, J. L., McIntire, T. M., Milton, S. C., Cotman, C. W., and Glabe, C. G. (2003) *Science* **300,** 486–489
21. Chien, P., Weissman, J. S., and DePace, A. H. (2004) *Annu. Rev. Biochem.* **73,** 617–656
22. Tanaka, M., Chien, P., Naber, N., Cooke, R., and Weissman, J. S. (2004) *Nature* **428,** 323–328
23. King, C. Y., and Diaz-Avalos, R. (2004) *Nature* **428,** 319–323
24. Tycko, R. (2003) *Biochemistry* **42,** 3151–3159
25. Burkoth, T. S., Benzinger, T. L. S., Urban, V., Morgan, D. M., Gregory, D. M., Thiyagarajan, P., Botto, R. E., Meredith, S. C., and Lynn, D. G. (2000) *J. Am. Chem. Soc.* **122,** 7883–7889
26. Balbach, J. J., Ishi, Y., Antzutkin, O. N., Leapman, R. D., Rizzo, N. W., Dyda, F., Reed, J., and Tycko, R. (2000) *Biochemistry* **39,** 13748–13759
27. Lansbury, P. T., Jr., Costa, P. R., Griffiths, J. M., Simon, E. J., Auger, M., Halverson, K. J., Kocisko, D. A., Hendsch, Z. S., Ashburn, T. T., Spencer, R. G., Tidor, B., and Griffin, R. G. (1995) *Nat. Struct. Biol.* **2,** 990–998
28. Petkova, A. T., Buntkowsky, G., Dyda, F., Leapman, R. D., Yau, W. M., and Tycko, R. (2004) *J. Mol. Biol.* **335,** 247–260
29. Tycko, R. (2004) *Curr. Opin. Struct. Biol.* **14,** 96–103
30. Eckenhoff, R. G., Johansson, J. S., Wei, H., Carnini, A., Kang, B., Wei, W., Pidikiti, R., Keller, J. M., and Eckenhoff, M. F. (2004) *Anesthesiology* **101,** 703–709
31. Jarrett, J. T., Berger, E. P., and Lansbury, P. T., Jr. (1993) *Biochemistry* **32,** 4693–4697
32. Walsh, D. M., Lomakin, A., Benedek, G. B., Condron, M. M., and Teplow, D. B. (1997) *J. Biol. Chem.* **272,** 22364–22372
33. Wood, S. J., Maleeff, B., Hart, T., and Wetzel, R. (1996) *J. Mol. Biol.* **256,** 870–877
34. Harper, J. D., Wong, S. S., Lieber, C. M., and Lansbury, P. T., Jr. (1999) *Biochemistry* **38,** 8972–8980
35. Nichols, M. R., Moss, M. A., Reed, D. K., Lin, W.-L., Mukhopadhyay, R., Hoh, J. H., and Rosenberry, T. L. (2002) *Biochemistry* **41,** 6115–6127
36. O'Nuallain, B., Williams, A. D., Westermark, P., and Wetzel, R. (2004) *J. Biol. Chem.* **279,** 17490–17499
37. Terzi, E., Holzemann, G., and Seelig, J. (1997) *Biochemistry* **36,** 14845–14852
38. Choo-Smith, L. P., Garzon-Rodriguez, W., Glabe, C. G., and Surewicz, W. K. (1997) *J. Biol. Chem.* **272,** 22987–22990
39. Choo-Smith, L. P., and Surewicz, W. K. (1997) *FEBS Lett.* **402,** 95–98
40. Kakio, A., Nishimoto, S., Yanagisawa, K., Kozutsumi, Y., and Matsuzaki, K. (2002) *Biochemistry* **41,** 7385–7390
41. Nichols, M. R., Moss, M. A., Reed, D. K., Hoh, J. H., and Rosenberry, T. L. (2005) *Biochemistry*, **44,** 165–173
42. Buck, M. (1998) *Q. Rev. Biophys.* **31,** 297–355
43. Fezoui, Y., and Teplow, D. B. (2002) *J. Biol. Chem.* **277,** 36948–36954
44. Li, H. T., Du, H. N., Tang, L., Hu, J., and Hu, H. Y. (2002) *Biopolymers* **64,** 221–226
45. Padrick, S. B., and Miranker, A. D. (2002) *Biochemistry* **41,** 4694–4703
46. Means, G. E. (1977) *Methods Enzymol.* **47,** 469–478
47. Sreerama, N., and Woody, R. W. (2000) *Anal. Biochem.* **287,** 252–260
48. Debye, P. (1947) *J. Phys. Colloid Chem.* **51,** 18–32
49. Zimm, B. H. (1948) *J. Chem. Phys.* **16,** 1093–1099
50. Tseng, B. P., Esler, W. P., Clish, C. B., Stimson, E. R., Ghilardi, J. R., Vinters, H. V., Mantyh, P. W., Lee, J. P., and Maggio, J. E. (1999) *Biochemistry* **38,** 10424–10431
51. LeVine, H. (1993) *Protein Sci.* **2,** 404–410
52. Zagorski, M. G., Yang, J., Shao, H., Ma, K., Zeng, H., and Hong, A. (1999) *Methods Enzymol.* **309,** 189–204
53. Jarrett, J. T., and Lansbury, P. T., Jr. (1993) *Cell* **73,** 1055–1058
54. Gursky, O., and Aleshkov, S. (2000) *Biochim. Biophys. Acta* **1476,** 93–102
55. Barrow, C. J., Yasuda, A., Kenny, P. T., and Zagorski, M. G. (1992) *J. Mol. Biol.* **225,** 1075–1093
56. LeVine, H., III (2002) *Arch. Biochem. Biophys.* **404,** 106–115
57. Soto, C., and Frangione, B. (1995) *Neurosci. Lett.* **186,** 115–118
58. Walsh, D. M., Hartley, D. M., Kusumoto, Y., Fezoui, Y., Condron, M. M., Lomakin, A., Benedek, G. B., Selkoe, D. J., and Teplow, D. B. (1999) *J. Biol. Chem.* **274,** 25945–25952
59. Lashuel, H. A., Hartley, D. M., Petre, B. M., Wall, J. S., Simon, M. N., Walz, T., and Lansbury, P. T. J. (2003) *J. Mol. Biol.* **332,** 795–808
60. Goldsbury, C. S., Wirtz, S., Muller, S. A., Sunderji, S., Wicki, P., Aebi, U., and Frey, P. (2000) *J. Struct. Biol.* **130,** 217–231
61. Esler, W. P., Stimson, E. R., Jennings, J. M., Vinters, H. V., Ghilardi, J. R., Lee, J. P., Mantyh, P. W., and Maggio, J. E. (2000) *Biochemistry* **39,** 6288–6295
62. Myszka, D. G., Wood, S. J., and Biere, A. L. (1999) *Methods Enzymol.* **309,** 386–402
63. Hasegawa, K., Ono, K., Yamada, M., and Naiki, H. (2002) *Biochemistry* **41,** 13489–13498
64. Sengupta, P., Garai, K., Sahoo, B., Shi, Y., Callaway, D. J. E., and Maiti, S. (2003) *Biochemistry* **42,** 10506–10513
65. Harper, J. D., and Lansbury, P. T., Jr. (1997) *Annu. Rev. Biochem.* **66,** 385–407
66. Naiki, H., and Nakakuki, K. (1996) *Lab. Invest.* **74,** 374–383
67. Andreu, J. M., and Timasheff, S. N. (1986) *Methods Enzymol.* **130,** 47–59
68. Yoshida, K., Yamaguchi, T., Adachi, T., Otomo, T., Matsuo, D., Takamuku, T., and Nishi, N. (2003) *J. Chem. Phys.* **119,** 6132–6142
69. Sikorski, P., Atkins, E. D., and Serpell, L. C. (2003) *Structure* (*Camb.*) **11,** 915–926
70. Chan, W., Fornwald, J., Brawner, M., and Wetzel, R. (1996) *Biochemistry* **35,** 7123–7130